Plasma Physics and Controlled Fusion

PAPER

Modeling active control of resistive wall mode with power saturation and sensor noise on HL-2M

To cite this article: S Wang *et al* 2021 *Plasma Phys. Control. Fusion* **63** 055019

IOP Publishing Plasma Physics and Controlled Fusion
Plasma Phys. Control. Fusion **63** (2021) 055019 (12pp) https://doi.org/10.1088/1361-6587/abf315

Modeling active control of resistive wall mode with power saturation and sensor noise on HL-2M

S Wang[1,*], Y Q Liu[2,*], G L Xia[3], X M Song[1], G Z Hao[1], L Li[4], B Li[1], N Zhang[1], G Q Dong[1], X Bai[1] and G Y Zheng[1]

[1] Southwestern Institute of Physics, PO Box 432, Chengdu 610041, People's Republic of China
[2] General Atomics, PO Box 85 608, San Diego, CA 92186-5608, United States of America
[3] CCFE, Culham Science Centre, Abingdon OX14 3DB, United Kingdom
[4] Donghua University, College of Science, Shanghai 201620, People's Republic of China

E-mail: wangs@swip.ac.cn and liuy@fusion.gat.com

Received 30 December 2020, revised 2 March 2021
Accepted for publication 29 March 2021
Published 16 April 2021

Abstract

The resistive wall mode (RWM) control on the HL-2M tokamak is simulated with the MARS-F code (Liu *et al* 2000 *Phys. Plasmas* **7** 3681), aiming at quantifying control current and voltage requirements when more realistic issues are taken into account, i.e. the control power saturation and the sensor signal noise. The fluid model predicts a narrow stability region for the $n = 1$ RWM without magnetic feedback, in the 2D parameter space of the plasma pressure versus the toroidal flow speed. Magnetic feedback can fully stabilize the RWM on HL-2M. Without considering the voltage limitation and the sensor signal noise, it is found that plasma flow helps active control of the mode, by reducing the required critical feedback gain for both flux-to-current and flux-to-voltage control schemes. In the absence of the sensor signal noise, the lowest control voltage saturation level, below which the RWM control is lost, is found to roughly satisfy a linear relation to the plasma flow frequency, indicating that subsonic plasma flow is effective in relaxing the control power requirement for the RWM feedback stabilization. The presence of the sensor signal noise substantially modifies the feedback results. A statistical study finds that the sensor signal noise, with the standard deviation of 0.1 G on HL-2M, roughly doubles the required control voltage for successful mode control. The synergistic stabilization effect due to plasma flow is somewhat weakened by the presence of the sensor signal noise. At a given rotation, the tolerable voltage limit generally increases with increasing feedback gain due to the sensor signal noise.

Keywords: resistive wall mode, active control, power saturation, HL-2M

(Some figures may appear in colour only in the online journal)

1. Introduction

The resistive wall mode (RWM) is one of the major instabilities of concern in advanced tokamak (AT) scenarios, which aim at steady state and high performance operations. Steady-state operation requires fully non-inductive current drive including maximization of the bootstrap current fraction, which in turn requires high plasma pressure [1]. For this reason, the AT scenarios are often designed to have the plasma pressure exceeding the Troyon no wall limit [2], resulting in unstable ideal external kink and RWM. An unstable RWM may cause major disruption of the tokamak plasma discharge, since it cannot easily non-linearly saturate by itself. Extensive experimental and theoretical studies have shown that the RWM can be stabilized by plasma flow in conjunction with various passive

* Authors to whom any correspondence should be addressed.

free energy dissipation mechanisms [3–13] and/or magnetic feedback [14–31] in tokamak devices. Much work has also been performed on revised filed pinch devices, in particular with significant success regarding active control of the RWM in experiments [32–36]. The fluid model has shown remarkable agreement with experimental results in both the mode stability and active control [37, 38].

This work specifically focuses on numerical investigation of the RWM stability on the HL-2M tokamak. HL-2M is a medium-sized copper-conductor tokamak [39, 40], with the design (maximal) plasma current of $I_p = 2.5$ (3) MA, toroidal field $B_0 = 2.2$ (3) T, major radius $R_0 = 1.78$ m, minor radius $a = 0.65$ m, and elongation $\kappa = 1.8$. In HL-2M, the up-down symmetric poloidal field coil system is located between the toroidal field coils and the vacuum vessel, allowing flexibility of operating in various divertor configurations including the snowflake configurations [41]. One of the key objectives of the HL-2M design is to study high beta, high performance fusion plasmas. The first plasma has recently been successfully produced on this device. Controlling the RWM instability is one of the main research topics in HL-2M during the later phase of operation. This motivates our present modeling work, where we consider both passive and active control of the RWM for a reference, high-beta target plasma designed on HL-2M.

Previous studies have shown that combination of passive stabilization and active control provides an effective way to suppress the RWM [42–44]. In particular, reference [44] investigated the combined effects of toroidal plasma flow, drift kinetic effects from thermal particles, and magnetic feedback on the RWM stability in an HL-2M plasma. Drift kinetic stabilization is ignored in this work, by two reasons. First, this work aims at a conservative estimate of the control power requirements for HL-2M. Since the kinetic contribution provides additional stabilization to the RWM in HL-2M [44], we obtain the worst-scenario results, in terms of the control requirements, by neglecting kinetic effects. Secondly, drift kinetic stabilization of the RWM sensitively depends on the assumed plasma toroidal rotation frequency, with the latter being difficult to be accurately predicted for HL-2M. A more realistic modeling of the control requirements, including the kinetic effects, may therefore be more valuable when the toroidal flow can be directly measured in the future HL-2M high performances discharges.

This work instead focuses more on the control aspects that were neglected in the previous work. As we shall show, inclusion of these extra elements results in new physics effects on the RWM stability. More importantly, the present study presents an important step towards realistic modeling of the RWM control on HL-2M. The new physics effects considered in this work include:

- Effect of power saturation on the active control system, where we investigate what happens to the RWM feedback, if the power supply limit is reached in future experiments.
- Effect of sensor signal noise on the control system, where we focus on the high-frequency white noise with Gaussian characteristics.
- Quantitative comparison of the active control performance between the so-called flux-to-voltage and flux-to-current control schemes.
- Initial value simulation of the close-loop system with or without assuming toroidal equilibrium flow of the plasma, allowing quantification of the control voltage and current requirements for the RWM feedback on HL-2M. This is different from the eigenvalue approach taken in the previous work [44].

We note that similar initial value simulations for the RWM control have previously been carried out for a JET-like plasma [30] and for the international thermonuclear experimental reactor (ITER) 9 MA advanced scenario [31], but assuming vanishing plasma equilibrium flow. This work presents the first numerical study of the synergistic effect by both magnetic feedback and plasma flow on the RWM stability, in the presence of control power saturation and sensor signal noise. We also note that the sensor noise issue has partially been studied in previous work [20, 23–25, 27] but without considering the voltage saturation. As for the modeling tool, we utilize the MARS-F code [15] updated to accommodate initial value simulations for close-loop control systems.

The remainder of the paper is organized as follows. Section 2 briefly introduces the magneto-hydrodynamic (MHD) and control models in MARS-F. Section 3 reports numerical results on passive and active control, as well as the combination of both, on the RWM stability on HL-2M. We draw conclusion in section 4.

2. Computational model

The MARS-F code is adopted to compute the growth rate of the RWM and to solve the feedback equation. In this work, we describe the RWM by an ideal MHD model:

$$(\tilde{\gamma} + in\Omega)\xi = \mathbf{v} + (\xi \cdot \nabla\Omega)R^2\nabla\phi \tag{1}$$

$$\rho(\tilde{\gamma} + in\Omega)\mathbf{v} = -\nabla p + \mathbf{j}\times\mathbf{B} + \mathbf{J}\times\mathbf{b} - \rho[2\Omega\hat{\mathbf{Z}}\times\mathbf{v} + (\mathbf{v}\cdot\nabla\Omega)R^2\nabla\phi] - \nabla\cdot\Pi \tag{2}$$

$$(\tilde{\gamma} + in\Omega)\mathbf{b} = \nabla\times(\mathbf{v}\times\mathbf{B}) + (\mathbf{b}\cdot\nabla\Omega)R^2\nabla\phi \tag{3}$$

$$(\tilde{\gamma} + in\Omega)p = -(\mathbf{v}\cdot\nabla)P - \Gamma P\nabla\cdot\mathbf{v} \tag{4}$$

$$\mu_0\mathbf{j} = \nabla\times\mathbf{b}, \tag{5}$$

where $\tilde{\gamma} = \gamma + i\omega_r$ is the eigenvalue of the mode, to be corrected by a Doppler shift frequency $in\Omega$ associated with toroidal flow of the plasma. Here, n is the toroidal mode number and Ω the plasma rotation frequency along the toroidal angle ϕ. Quantities in lower case, $(\xi, \mathbf{v}, \mathbf{j}, \mathbf{b}, p)$, denote the plasma displacement, the perturbed velocity, current, magnetic field and plasma pressure, respectively. The upper case quantities

$(\mathbf{B},\mathbf{J},P)$ denote the plasma equilibrium magnetic field, current, and pressure, respectively. Other quantities include the plasma equilibrium mass density ρ, the plasma major radius R, the unit vector in the vertical direction $\hat{\mathbf{Z}}$.

The viscous stress tensor Π represents the ion-Landau damping physics on the RWM [4], with $\nabla\cdot\Pi=\kappa_{//}\sqrt{\pi}|k_{//}|v_{th}^{i}|\rho\mathbf{v}_{//}\hat{\mathbf{b}}\hat{\mathbf{b}}$. Here, $\kappa_{//}$ is a numerical coefficient specifying the damping strength. $k_{//}$ is the parallel wave number, v_{th}^{i} the ion thermal velocity, $\mathbf{v}_{//}$ the perturbed parallel velocity of the plasma, and $\hat{\mathbf{b}}=\mathbf{B}/B$.

The MARS-F code directly solves the above perturbed MHD equations in the plasma region, together with the following feedback equation in the vacuum region outside the plasma:

$$\frac{d\Psi_f}{dt}+R_fI_f=V_f=-Gb_s, \tag{6}$$

where Ψ_f is the perturbed magnetic flux through the active coils. I_f,R_f,V_f are the current, resistance and voltage of the active coils, respectively. G is the feedback gain which generally takes complex values. In the MARS-F formulation and throughout this paper, G is normalized by R_0^2/τ_A, rendering the feedback gain a dimensionless quantity. b_s is the sensor signal, defined as the point-wise poloidal magnetic field perturbation in this work.

The above control logic, referred to as the flux-to-voltage control, applies to linear close-loop systems. In more general cases, where the control voltage V_f is constrained by the voltage limitation $V_f^{\rm lim}$, we assume:

$$V_f=\begin{cases} V_f^{\rm lim}, & \text{if} \quad V_f\geqslant V_f^{\rm lim}\\ -V_f^{\rm lim}, & \text{if} \quad V_f\leqslant -V_f^{\rm lim}\\ -Gb_s, & \text{if} \quad |V_f|<V_f^{\rm lim}. \end{cases} \tag{7}$$

Furthermore, in the presence of the sensor signal noise, we assume $b_s=b_s^0+b_s^{\rm noise}$, where the noise contribution $b_s^{\rm noise}$ satisfies Gaussian distribution $N(0,\sigma^2)$ with zero mean and standard deviation of σ. The latter is a parameter that we shall scan in our initial value simulations.

Before showing numerical results, we remark that equation (6) is effectively converted into the flux-to-current control logic by neglecting the first term in the left hand side. This is what we shall employ when compare the two control schemes later on.

3. Numerical results

In what follows, we consider an AT plasma scenario designed for HL-2M, with the target plasma chosen as the original design of the HL-2M reference equilibrium for the high-β scenario, reaching the normalized beta value of $\beta_N\equiv\beta(\%)a(\mathrm{m})B_0(\mathrm{T})/I_p(\mathrm{MA})=4.31$. Here, β is the plasma pressure normalized by the toroidal magnetic pressure, $a=0.59$ m the plasma minor radius, $B_0=2.2$ T the vacuum toroidal magnetic field at the major radius of 1.78 m, and $I_p=2$ MA the plasma current. Note that the target equilibrium chosen in [44] has 10% higher plasma pressure than the reference one. Our target equilibrium exceeds the no-wall beta limit of $\beta_N^{\rm NW}=3.49$ for the onset of the $n=1$ ideal external kink instability, but is below the ideal-wall limit of $\beta_N^{\rm IW}=5.5$. Defining the pressure scaling factor $C_\beta\equiv(\beta_N-\beta_N^{\rm NW})/(\beta_N^{\rm IW}-\beta_N^{\rm NW})$, the target plasma corresponds to $C_\beta\sim 0.4$.

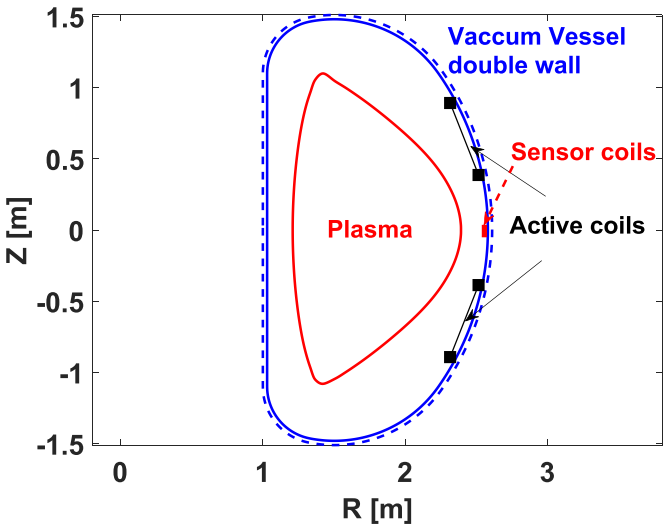

Figure 1. Basic geometry of the RWM control on HL-2M: the plasma boundary shape (red solid line) for a 2 MA double-null equilibrium from the high performance scenario, the shape of the conducting vacuum vessel with double-wall structure (blue solid and dashed lines), the locations of the active (black dots) and sensor (red dot) coils. The poloidal angle of the center of the active coils is $|\theta_c|=29.9^\circ$, with the poloidal coverage of $\Delta\theta=21.8^\circ$.

We also note that the beta limits reported above are close to, but not exactly the same as, those computed in the previous work [44]. This is because slightly different procedures are employed in computing the beta limits. In this work, the edge safety factor value is fixed (at $q_a=5.75$, being the same as that of the reference equilibrium) when scanning the plasma pressure for beta limit computations. The total plasma current is instead fixed in the previous work [44] while scanning the plasma pressure.

The plasma boundary shape and the wall shape are shown in figure 1. Considered here is a double-null plasma configuration. On HL-2M, the vacuum vessel, with a double-shell structure, are located at the normalized radii of $d/a=1.30,1.35$, respectively. This serves as the main conducting structure and is used as the resistive wall throughout this study. Each vessel shell is made of 5 mm thick Inconel 625 material with resistivity of 1.29 $\mu\Omega\cdot$m [40]. The wall time (the slowest $n=1$ eddy current decay time) is calculated to be $\tau_w^{inner}=1.26\times10^4\,\tau_A$ for the inner wall and $\tau_w^{outer}=1.31\times10^4\,\tau_A$ for the outer wall. The effective wall time of the double-shell is calculated to be $\tau_w=2.2\times10^4\,\tau_A$.

The RWM feedback system consists of two sets of active coils and one set of sensor coils, both located at the low field side just inside the inner wall. As preliminary designed on HL-2M, the poloidal angle of the center of each set of active coils is $|\theta_c|=29.9^\circ$ (as measured in geometric poloidal angle θ), with the poloidal coverage of $\Delta\theta=21.8^\circ$. The sensor coils

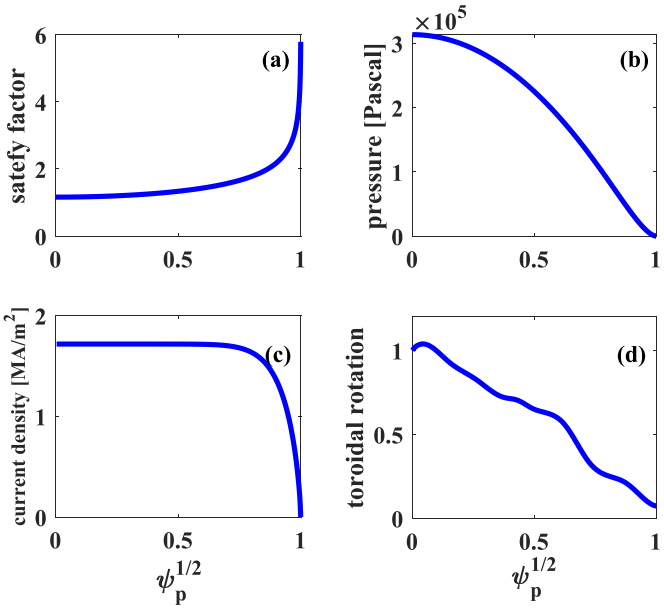

Figure 2. The equilibrium radial profiles. Shown are the (a) the safety factor profile, (b) the plasma pressure, (c) the surface averaged toroidal current density and (d) the toroidal rotation frequency chosen for the modeling in HL-2M, the on-axis value of the rotation is normalized to unity here. The radial coordinate is labeled by $\sqrt{\psi_p}$, with ψ_p being the normalized equilibrium poloidal flux.

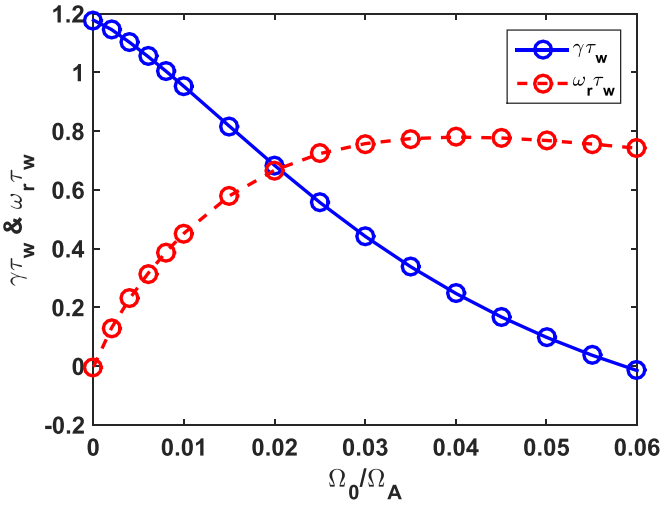

Figure 3. The MARS-F computed open-loop growth rate (solid line) and mode frequency (dashed line) of the $n = 1$ RWM, with varying on-axis toroidal rotation frequency Ω_0 (normalized by the Alfvén frequency Ω_A) while fixing the overall rotation profile as shown in figure 2. Considered here is the target equilibrium ($C_\beta = 0.4$) designed on HL-2M. The parallel viscosity coefficient is assumed to be $\kappa_{//} = 1.5$. The double-wall radial locations are assumed as $d/a = 1.30$ and 1.35.

are located at the outboard mid-plane measuring the perturbation in the poloidal field component. This choice is motivated by the well established result that the internal poloidal sensors perform much superior over the radial sensors for the RWM control [15, 45]. Note that in this study, the single set of sensor measures both the amplitude and toroidal phase of the perturbed field, which in turn are used to drive the coil currents in both the upper and lower rows of control coils via two independent feedback gains. This can be viewed as a multi-input-multi-output (MIMO) control scheme following experimental traditions [32, 46, 47].

The choice of the radial location (i.e. in-vessel) for active coils here follows that in ITER, where magnetic coils are designed to control the edge localized mode (ELM) and the RWM. Compared to a design where the active coils are located outside the vacuum vessel, the in-vessel coils offer better coupling of the control field to the plasma. In particular, the overall time lag of the close-loop system is reduced by avoiding the field penetration through the wall. On the other hand, the obvious disadvantages of the in-vessel coil design, in particular for future fusion reactors, are the space constraint and the irradiation problem. These are not severe issues though for HL-2M.

Figure 2 plots the radial profiles for the safety factor q, plasma pressure P, averaged toroidal current density J_ϕ and the plasma toroidal rotation frequency Ω. The safety factor at the plasma edge (for the limiter-like plasma considered here) is $q_a = 5.75$, and the value is fixed when scanning the plasma pressure as mentioned before. The pressure shown in figure 2 (b) corresponds to the reference equilibrium, with the pressure scaling factor of $C_\beta \sim 0.4$. The on-axis value of the rotation frequency Ω is normalized to unity.

3.1. RWM stabilization by plasma flow

The open-loop stability problem for the RWM is simulated in this part, taking into account the plasma flow effect. We first consider the target equilibrium with $C_\beta \sim 0.4$. In what follows, we shall scan the on-axis rotation amplitude while fixing the overall radial profile shape as shown in figure 2 (d). The toroidal flow amplitude is estimated to be in the order of 10^5 rad s^{-1}, given the available neutral beam injection power on HL-2M.

Figure 3 reports the MARS-F computed growth rate $\gamma\tau_w$ and real frequency $\omega_r\tau_w$ of the $n = 1$ RWM in the target plasma, while scanning the on-axis rotation frequency Ω_0. The latter is normalized by the toroidal Alfvén frequency $\Omega_A = v_A/R_0$ with $v_A \equiv B_0/\sqrt{\mu_0\rho_0}$, where μ_0 is the permeability of free space and ρ_0 the mass density at the center of the plasma. A strong parallel sound wave damping model is adopted here, with the damping coefficient $\kappa_{//} = 1.5$. We remark that there is no unique value for $\kappa_{//}$. It has previously been thought that $\kappa_{//} \ll 1$ when the plasma toroidal flow speed is well below the sound speed [48]. On the other hand, there are regions close to resonant surfaces where the parallel phase velocity in the plasma frame is large enough to resonate with thermal particles, and where the local damping is strong [49]. The large value of $\kappa_{//}$ used here mimics strong ion Landau damping. According to the fluid RWM theory, the critical rotation for the mode stabilization depends on this damping coefficient [50].

Figure 3 shows that the critical on-axis rotation for the RWM stabilization is about 6% of the Alfvén frequency on

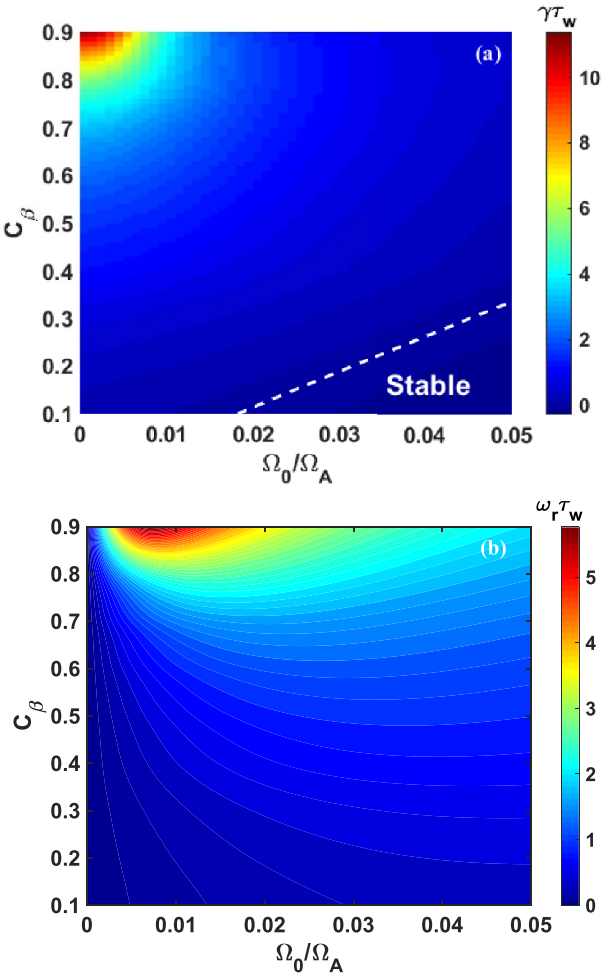

Figure 4. Contour plots of (a) growth rate, and (b) mode frequency, of the MARS-F computed open-loop $n = 1$ RWM, in the 2D parameter space of the on-axis toroidal rotation frequency Ω_0 and the equilibrium pressure scaling factor C_β. The dashed white line in (a) indicates the stability boundary. The parallel viscosity coefficient is assumed to be $\kappa_{//} = 1.5$. The double-wall radial locations are assumed as $d/a = 1.30$ and 1.35, respectively.

HL-2M, assuming the ideal MHD model. This value is consistent with the findings from [3] and [4]. We emphasize, however, that the critical rotation is significantly altered by considering the drift kinetic stabilization of the RWM due to thermal particles, as has already been demonstrated in [44] for HL-2M. By neglecting the drift kinetic effects in this study, we obtain more conservative prediction for the RWM instability on HL-2M, as long as the passive stabilization is concerned.

Next, we expand the parametric study reported in figure 3, by considering a family of equilibria obtained with the pressure scaling factor C_β. This leads to a 2D parameter scan in the $C_\beta - \Omega_0/\Omega_A$ space, with the computed stability results reported in figure 4. The RWM growth rate rapidly increases with C_β as the latter approaches 1 (the ideal-wall beta limit). Passive stabilization alone, by the plasma flow, becomes more difficult at higher plasma pressures. In fact, only a narrow window exists in this 2D parameter space, where the RWM instability is fully suppressed (again according to the fluid theory) on HL-2M. The marginal stability curve, plotted as the white dashed line in figure 4(a), is well approximated by a linear relation $\Omega_0/\Omega_A = 0.152\ C_\beta$, quantifying the required critical rotation speed for the RWM stabilization on HL-2M, as the plasma pressure is increased. On the other hand, we also note that the sub-sonic toroidal flow is generally effective in reducing the mode growth rate even at high C_β. For instance, at $C_\beta = 0.9$, the normalized mode growth rate $\gamma\tau_w$ is reduced from 11.38 to 1.67, as the on-axis rotation frequency Ω_0/Ω_A increases from 0 to 0.02.

Figure 4(b) shows that the mode frequency is almost the same order as the RWM growth rate, and generally scales with C_β. For relatively low C_β equilibria, the mode frequency monotonically increases with the plasma rotation speed, while it becomes non-monotonic in cases with higher C_β values.

3.2. RWM stabilization by feedback control: eigenvalue approach

Feedback stabilization of the $n = 1$ RWM on HL-2M is investigated in this part, following the eigenvalue approach which can only be employed to study linear control problem. Different from the previous work [44], we shall consider and compare two control schemes, i.e. the flux-to-voltage versus the flux-to-current control. The latter is what was assumed in [44].

With a MIMO control system, it is important to choose the phase of the (complex) feedback gains associated with the upper and lower rows of the active coils. As shown in figure 5, at a given gain amplitude ($|G| = 0.3$) for both rows of active coils, the close-loop growth rate is sensitive to the choice of the gain phase. Feedback has almost no effect on the mode stabilization (compared to the open-loop value as reported in figure 3), if the gain phase is not properly chosen. The optimal gain phase is $\phi_U = -\phi_L = 120°$ for the case shown in figure 5, where we have assumed the flux-to-voltage control scheme. Interestingly, the same optimal gain phase was found with the flux-to-current control scheme [44]. We also mention that the optimal gain phase is generally not sensitive to the gain amplitude $|G|$ but can be altered by the toroidal plasma flow. A vanishing equilibrium flow is assumed in figure 5.

Next, fixing the feedback gain phase to the optimal value as found from figure 5, we investigate the RWM stabilization with increasing gain amplitude. Figure 6 compares the feedback performance between the two control schemes as mentioned before. The open-loop growth rate (at $|G| = 0$) of the RWM is lower in the flux-to-voltage control scheme as compared to the flux-to-current control. This is because in the former, the active coils act as additional passive conductors (on top of the resistive wall), reducing the mode growth rate. A systemically study of this additional passive stabilization mechanism, where the relative conductivities between the active coils and the resistive wall were scanned, was reported in [31].

We note that the close-loop growth rates converge to the same value between the two control schemes, as we increase the feedback gain amplitude as shown in figure 6. This can be analytically understood. Indeed, equation (6) shows that the critical feedback gain should be the same between the two

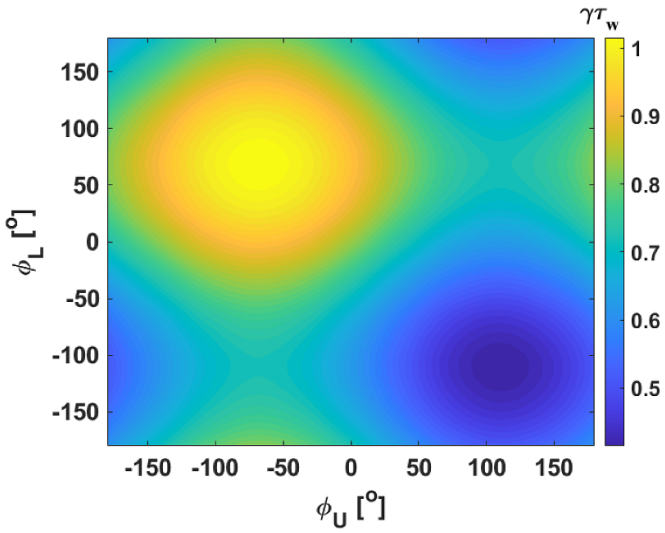

Figure 5. Contour plots of the growth rate of the close-loop $n = 1$ RWM, in the 2D parameter space of the feedback gain phase (ϕ_U, ϕ_L) for the upper and lower rows of active coils, respectively. Considered is the flux-to-voltage control scheme with the proportional gain amplitude fixed at $|G| = 0.3$. Assumed is vanishing equilibrium flow. Other parameters are the same as that in figure 3.

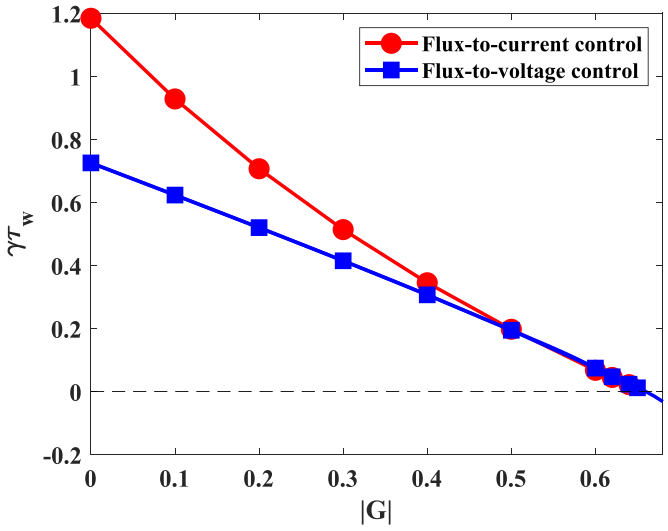

Figure 6. The MARS-F computed close-loop growth rate of the $n = 1$ RWM with increasing feedback gain amplitude $|G|$, for the target equilibrium ($C_\beta = 0.4$) designed on HL-2M. The phase of the feedback gains are fixed at $\phi_U = -\phi_L = 120^\circ$ for the upper and lower rows of active coils, respectively.

control schemes, since the first term from the left hand side of the equation disappears at the marginal stability point. This means that both control schemes yield the same critical gain value for the mode stabilization, as confirmed by figure 6. We emphasize that the above statement is valid only if the mode has vanishing real frequency at marginal stability point. Finite plasma flow induces finite mode frequency at the marginal stability point, and consequently will lead to different critical gain amplitude for the mode stabilization between the two control schemes. This will be demonstrated in the following sub-section.

3.3. Synergistic stabilization of RWM by feedback and plasma flow

Feedback stabilization of the RWM for the target HL-2M plasma is compared between the flux-to-voltage and flux-to-current control schemes in the presence of the plasma flow. Both the eigenvalue and initial value approaches are adopted in this sub-section.

Figure 7 compares the MARS-F computed close-loop growth rate between the two control schemes, while scanning the feedback gain amplitude assuming different toroidal rotation frequencies. The gain phase is fixed at the optimal values obtained assuming vanishing flow (figure 5). Despite the fact that the optimal gain phase is modified by the plasma flow [44], it is reasonable to fix the gain phase during feedback control in practice, even if the plasma rotation is evolving. Figure 7 shows that the RWM on HL-2M is fully stabilized when the feedback gain amplitude exceeds a critical value, $|G_{\rm cri}|$, with either control scheme. The critical gain value decreases with increasing plasma flow speed. On the other hand, at the same flow speed, the flux-to-voltage control scheme (figure 7 (b)) requires less critical gain than the flux-to-current scheme (figure 7 (a)), in order to stabilize the RWM.

The critical gain amplitude can be quantified for the target HL-2M plasma, as a function of the toroidal rotation frequency, by analytically fitting the numerical data shown in figure 7. We obtain $|G_{\rm cri}| = -38.6\ (\Omega_0/\Omega_A)^2 - 9.6\ \Omega_0/\Omega_A + 0.66$ for the flux-to-current control scheme and $|G_{\rm cri}| = -47.9\ (\Omega_0/\Omega_A)^2 - 11.5\ \Omega_0/\Omega_A + 0.66$ for the flux-to-voltage control. Note that these analytic fitting formulae recover the critical gain value at the limit of vanishing flow as reported in figure 6, as well as the critical rotation speed without feedback ($|G_{\rm cri}| = 0$) as shown in figure 3.

The eigenvalue approach reported above is good at obtaining the close-loop growth rate and the critical gain values for the mode stabilization, but does not reveal many quantities of practical importance for the RWM control, e.g. the required maximal control voltage and control current, the settling time for a stable control loop after the feedback is switched on, and more generally the overall dynamic behavior of the close-loop system. Initial value simulations are needed for these purposes, even for linear control. We note that some of the control loop characteristics, e.g. the maximal voltage and current requirements, can be recovered based on the eigenvalue approach, by performing inverse Laplace transform of the plasma response transfer function obtained with the eigenvalue approach [51]. This, however, requires the knowledge of open-loop transfer function, which can in principle be obtained with the Padé approximation of the numerically computed eigenvalue data [52]. Nevertheless, initial value simulations, though more time-consuming, offer direct information on the whole dynamics of the feedback system and is of more practical relevance too. In what follows, we focus on initial value simulations of the feedback system for the RWM control on HL-2M.

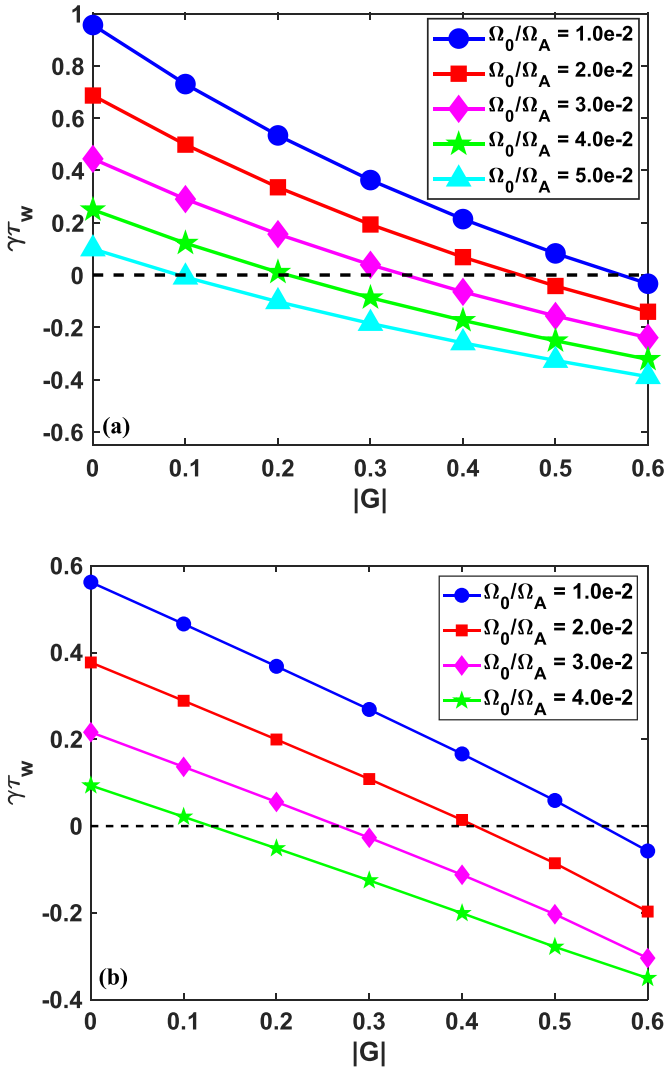

Figure 7. The MARS-F computed close-loop growth rate of the $n = 1$ RWM with increasing proportional gain amplitude, assuming (a) the flux-to-current control scheme and (b) the flux-to-voltage control scheme. Plotted are the different choices of the plasma toroidal rotation frequency. Other parameters are the same as that in figure 6.

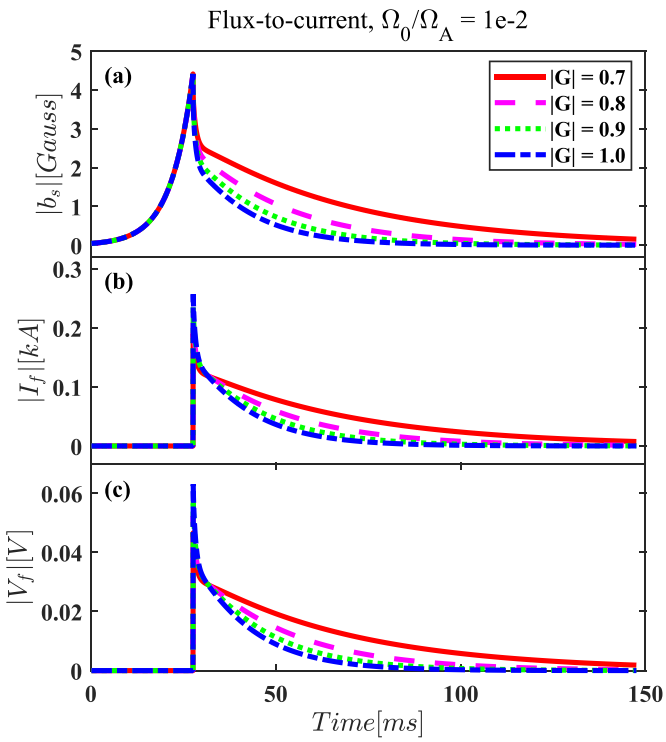

Figure 8. Simulated time traces of the $n = 1$ RWM feedback stabilization by the flux-to-current control scheme, in combination with the plasma toroidal flow. Plotted are the time traces of (a) the amplitude of the poloidal sensor signal, (b) the current amplitude in the active coils, and (c) the voltage of the active coil power supply. The control loop is closed at 25 ms. Different choices of feedback gain amplitude are plotted with different curve styles. The on-axis rotation frequency of $\Omega_0/\Omega_A = 0.01$. Other parameters are the same as that in figure 6.

The simulation results of linear control, without assuming control voltage limitation and sensor signal noise, are reported in figures 8 and 9, for the flux-to-current and flux-to-voltage control schemes, respectively. Note that it is the first time we report the initial value simulations with the flux-to-current scheme for the RWM control. With both control schemes, we vary the feedback gain $|G|$ from 0.7 to 1 while fixing the plasma flow speed at $\Omega_0/\Omega_A = 0.01$. These $|G|$ values are larger than the critical gain $|G_{\rm cri}|$, ensuring close-loop stability.

We first follow the open-loop stage for 25 ms with the flux-to-current control (figure 8) and 48 ms with the flux-to-voltage control scheme (figure 9), starting from the same initial perturbation amplitude as measured by the sensors (plots (a)). These open-loop time intervals allow the mode to exponentially grow to the same amplitude ($\sim$4.5 G) between the two schemes, when the control loop is closed. With the chosen gain values, the closed loops indeed become stable, with decreasing settling time at increasing feedback gain. Note that the dynamics of active coil current $I_f(t)$ (plots (b)) are qualitatively different between the two control schemes. At the time when the feedback is switched on, $I_f(t)$ continuously evolves with the flux-to-voltage control scheme. This is because with the latter scheme, control currents are already passively induced in the active coils in the open-loop stage.

Sharp decay of all control signals are found in figure 8 with the flux-to-current scheme, right after feedback is switched on. Both the maximal achievable control coil current and voltage are proportional to feedback gain with this scheme. This is not the case with the flux-to-voltage scheme. With the latter, the maximal control voltage increases with feedback gain as well, but the control coil current peaking value always stays the same (the peaking time varies though). For identical feedback gain, the maximal achievable voltage with the flux-to-voltage control is larger than that with the flux-to-current control.

With the flux-to-current control, both control current and voltage experience sudden jumps when the feedback is switched on. This has a significant implication for this control scheme. As has been analytically shown in [29], an upper limit cannot be imposed to the control current for the flux-to-current control scheme to ensure the close-loop stability. In other words, the control will be lost if the control current saturation is reached for this control scheme. Therefore, in the

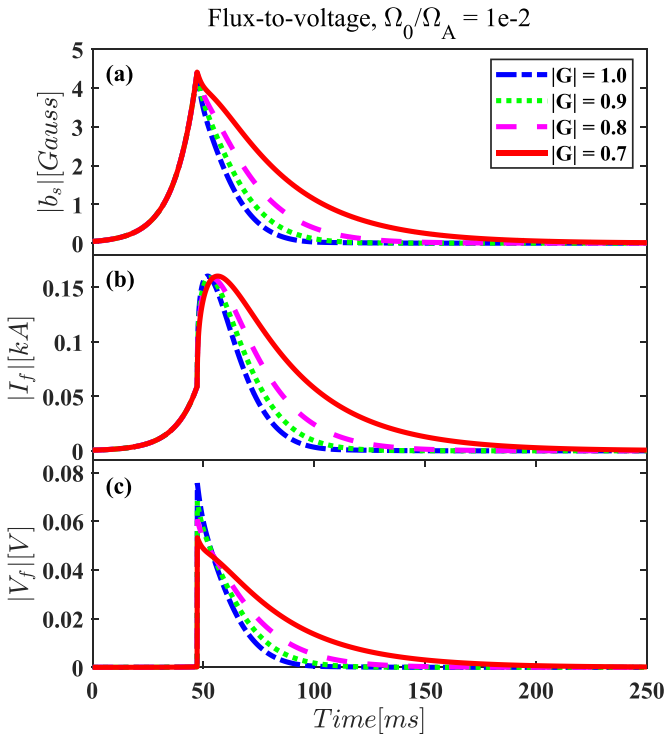

Figure 9. Simulated time traces of the $n = 1$ RWM feedback stabilization by the flux-to-voltage control scheme with the plasma toroidal flow effects. Plotted are the time traces of (a) the amplitude of the poloidal sensor signal, (b) the current amplitude in the active coils, and (c) the voltage of the active coil power supply. The control loop is closed at 48 ms. Different lines show the performances with different choices of feedback gain amplitude. Other parameters are the same as that in figure 8.

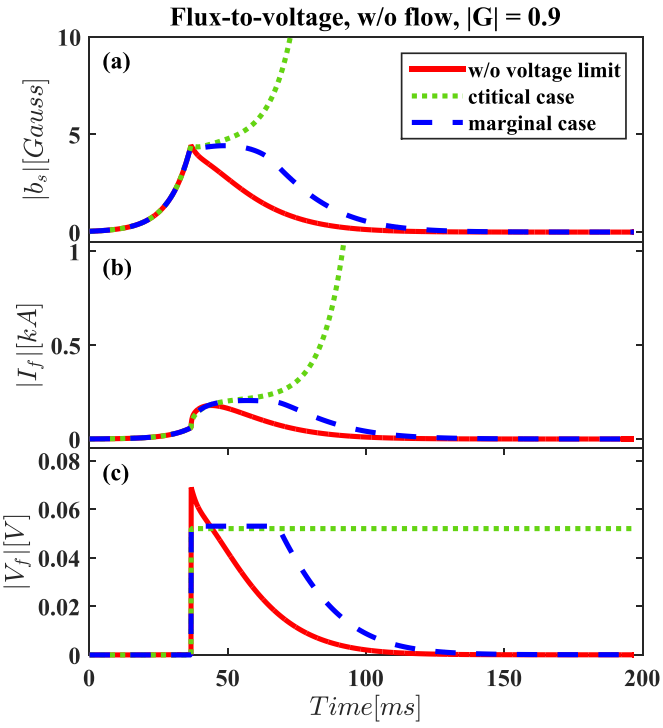

Figure 10. Comparison of three simulated time traces for the RWM with flux-to-voltage control scheme: linear feedback without control coil voltage limitation (red solid line), feedback with voltage limit just above (blue dashed line) and just below (green dotted line) the critical level. Plotted are the time traces of (a) the amplitude of the poloidal sensor signal, (b) the current amplitude in the active coils, and (c) the voltage of the active coil power supply. The control loop is closed at 37 ms. The proportional feedback gain is assumed as $|G| = 0.9$, the equilibrium is fixed at $C_\beta = 0.4$. No plasma flow effect is considered in these cases.

non-linear control to be studied below, we shall only consider the flux-to-voltage control scheme.

3.4. RWM control with power saturation and sensor noise

First, initial value simulations are performed, assuming the control voltage limitation $V_f^{\rm lim}$ for the active coils but in the absence of the sensor signal noise. Three examples are compared in figure 10. The solid curves indicate the linear control, where no voltage limit is imposed. In this case, the close-loop system achieves a maximal value of voltage, denoted as $V_f^{\rm max}$, as soon as feedback is switched on. $V_f^{\rm max}$ varies with feedback gain $|G|$ as shown in figure 9. Here, we have $V_f^{\rm max} = 0.07$ V at $|G| = 0.9$. It is evident that the feedback system will lose control when $V_f^{\rm lim}$ is below a critical value $V_f^{\rm min}$ ($= 0.054$ in this case). This critical case is shown by dotted curves in figure 10, where the control coil voltage saturates all the time and the close-loop RWM rapidly grows, i.e. the mode control is lost. For cases where $V_f^{\rm lim}$ is between $V_f^{\rm min}$ and $V_f^{\rm max}$, the RWM is eventually feedback stabilized despite the occurrence of temporary voltage saturation during the close-loop simulation. One such example is shown by dashed curves in figure 10. Finally, if the control voltage limit is larger than $V_f^{\rm max}$, the feedback system performs the same way as that without power saturation.

Shown in figure 10 are cases with vanishing plasma flow. We have also carried out similar simulations with finite plasma flow for the target HL-2M plasma. The key result of interest, i.e. the $V_f^{\rm min}$ value, is summarized in figure 11 versus the on-axis toroidal rotation frequency of the plasma. It is evident that the minimal control voltage needed to stabilize the RWM decreases with increasing plasma rotation. In other words, plasma flow helps to make the close-loop system more tolerable to the control voltage limitation. It is interesting that the minimal voltage requirement can be well represented by a linear fitting curve (dashed line in figure 11) $V_f^{\rm min} = -1.08\ \Omega_0/\Omega_A + 0.054$ for HL-2M. The fact that the proportionality coefficient here is an order one term indicates that the reduction of the minimal voltage is significant even with subsonic plasma flow.

Results reported in figure 10 are further expanded to other HL-2M equilibria with varying pressure. Figure 12 shows the $V_f^{\rm min}$ values in the 2D parameter space of both C_β and the plasma rotation Ω_0/Ω_A. The growth rate of the RWM is maximal as C_β approaches unity. The $V_f^{\rm min}$ value also reaches the maximum at this limit, especially in the absence of the plasma flow stabilization.

It is interesting to note that the $V_f^{\rm min}$ value is not always a monotonic function of C_β. For instance, at fixed flow speed

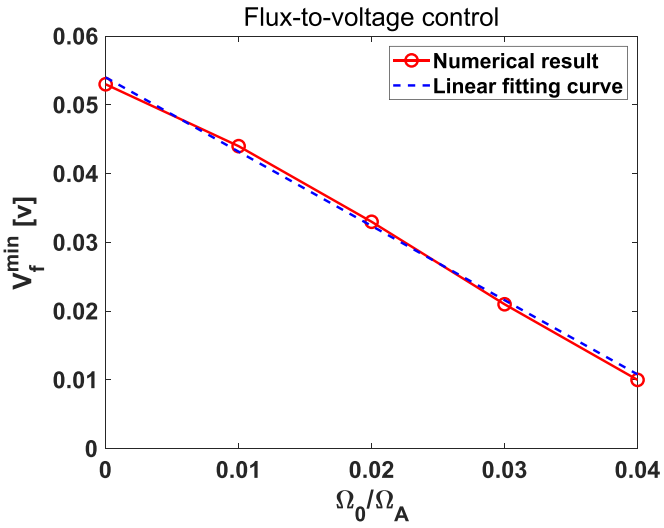

Figure 11. The required minimal voltage $V_f^{\min}$ versus the plasma toroidal rotation frequency. The computed (solid line) and analysis fitting (dashed line) curves are plotted. The other parameters are fixed at $C_\beta = 0.4, \kappa_{//} = 1.5, |G| = 0.9$.

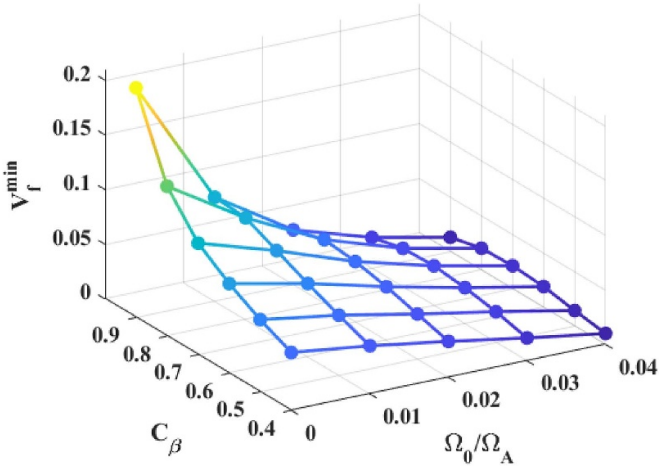

Figure 12. The MARS-F computed minimal voltage versus the normalized plasma rotation frequency. Here plasma pressure varies from $C_\beta = 0.4$ to 0.9. The other parameters are fixed at $\kappa_{//} = 1.5, |G| = 0.9$.

$\Omega_0/\Omega_A = 0.02$, we find that the $V_f^{\min}$ value at $C_\beta = 0.9$ is smaller than that at $C_\beta = 0.8$ or 0.7. Detailed examination reveals that this is related to the fact that close-loop time traces exhibit oscillating behavior (not shown here) at sufficiently fast plasma flow and at $C_\beta = 0.7$ or 0.8. On the contrary, the close-loop control voltage always monotonically decays with time at $C_\beta = 0.9$, independent of the rotation frequency.

As the final stage of study, we now also inject the Gaussian white noise into the sensor signal in the close-loop simulations. Figure 13 shows three examples of the simulated time traces for the close-loop system. All the input parameters are identical among these three cases, except the three different samples for the sensor noise (with the same standard deviation as shown in figure 13(d)) which are machine-generated during the simulations. The resulting close-loop performance,

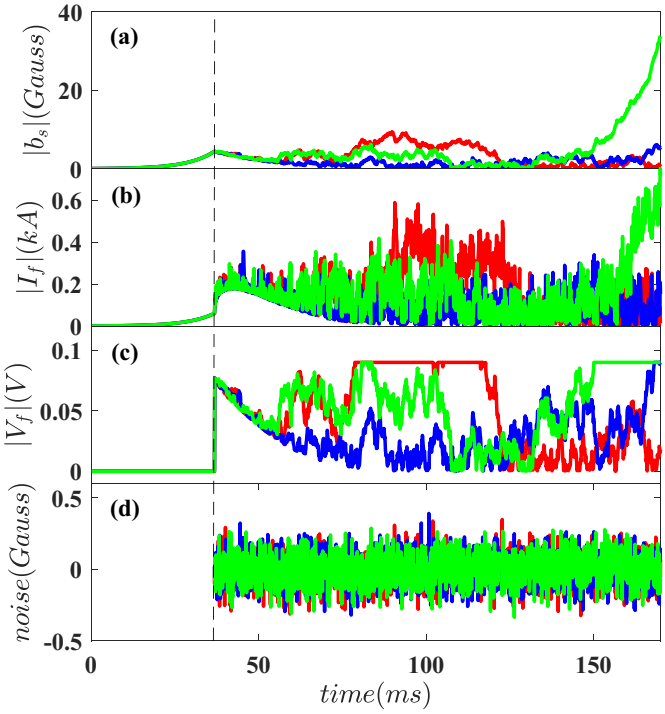

Figure 13. Three examples of initial value simulation of the $n = 1$ RWM feedback with control voltage saturation and sensor signal noise. All the input parameters are identical in these simulations, except that different samples of sensor signal noise are assumed. Plotted are (a) amplitude of the poloidal sensor signal, (b) the control coil current, (c) the control voltage, and (d) samples of the machine-generated noise with Gaussian distribution and standard deviation of $\sigma_{\text{noise}} = 0.1$ G. The feedback system closed at 37 ms. The other parameters are fixed at $C_\beta = 0.4, |G| = 1, \Omega_0 = 0$. The control voltage limit is set at $V_f^{\text{lim}} = 0.09$ V.

in the presence of the control voltage limitation, is however drastically different. In particular, in the case shown in green, the RWM control is eventually lost after about 150 ms simulation time. Without the control voltage limitation, the mode remains stable though the sensor noise does affect the control performance. Note that the sensor signal noise level is fixed in this study, with the standard deviation of $\sigma_{\text{noise}} = 0.1$ G following a multi-machine database analysis reported in [53].

We also note that the required voltage for controlling the RWM on HL-2M is generally small even in the presence of the sensor signal noise. The control voltage will certainly increase if we operate the AT plasma beyond the target pressure. Moreover, the busbar resistance and other resistant elements in the control circuit will further increase the overall power required for controlling the mode in real experiments. The required control coil current is about 0.6 kA according to figure 13(c) (again for the target plasma). The designed maximal current for the in-vessel magnetic coils is 10 kA on HL-2M. Preliminary estimate shows that ~5 kA current is needed to control type-I ELMs on HL-2M, utilizing the same set of in-vessel coils. This leaves a significant margin for the combined control of the ELM and the RWM on HL-2M. It should be noted that simultaneous control of ELMs and RWMs requires further modeling and experimental efforts to demonstrate the

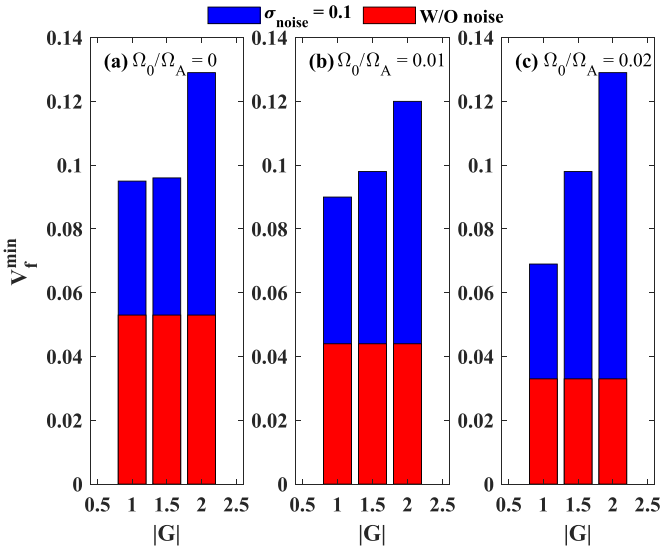

Figure 14. The minimal voltage $V_f^{\min}$ versus feedback gain in the presence of sensor noise for different plasma rotation frequencies: (a) without flow, (b) $\Omega_0/\Omega_A = 0.01$, (c) $\Omega_0/\Omega_A = 0.02$.
The minimal voltage needed to control the $n = 1$ RWM, in the absence of the sensor signal noise, is shown in red cubes.
The minimal voltage in the presence of sensor noise is evaluated from 20 initial value runs for each voltage limit, and the limit with 90% success rate (to stabilize the RWM) is defined as the minimal voltage $V_f^{\min}$. The plasma pressure is fixed at $C_\beta = 0.4$.

feasibility. The control power requirement and the potential interference/coupling between the ELM and RWM control are two major issues that need further investigation.

Figure 13 shows the statistic nature of the feedback system when the sensor signal noise is included and the control voltage is limited. To better quantity the results, we repeat 20 times the initial value simulation for each (deterministic) parameter setup, with different noise samples that have the same standard deviation. If the close-loop remains stable for 18 (i.e. 90%) out of 20 simulations, similar to those shown by red and blue curves in figure 13, we define the applied voltage limitation level as acceptable, or in other words the RWM control is successful with the given voltage limit.

Our eventual goal here is to identify the minimal voltage saturation level $V_f^{\min}$, above which the RWM control is still successful (in the above sense) in the presence of the sensor signal noise. Figure 14 compares the simulated $V_f^{\min}$ assuming three different plasma rotation frequencies. With each rotation, we also vary the feedback gain amplitude. In the absence of the sensor signal noise (histograms in red), much smaller values of $V_f^{\min}$ can be tolerated, where the RWM control is still successful. The $V_f^{\min}$ value decreases with increasing plasma flow, again indicating favorable stabilization effect brought in by the plasma flow. The $V_f^{\min}$ value however does not change with increasing feedback gain. This interesting result was also analytically demonstrated in [29].

With inclusion of the sensor signal noise (histograms in blue), we find three major changes. (1) The overall tolerable voltage limit is roughly doubled, compared to that without noise. (2) The plasma flow still generally plays a favorable role in reducing $V_f^{\lim}$, but this does not hold for all cases. Exceptions include the case with $|G| = 2$ and $\Omega_0/\Omega_A = 0.02$. (3) At a given rotation, the $V_f^{\min}$ value now depends on the feedback gain amplitude. Taking the extreme example shown in figure 14 (c), the $V_f^{\min}$ value at $|G| = 2$ is about twice of that at $|G| = 1$. This value (at $|G| = 2$) in turn is about four times larger than that without the sensor signal noise. The tolerable voltage limit is determined by two competing processes: favorable RWM stabilization with increasing feedback gain and feedback amplification of the sensor noise. The latter is the dominant factor responsible for the increasing tolerable voltage level. This is because, without sensor noise, the tolerable voltage level does not increase with feedback gain. Results from figure 14 thus show that for the RWM control on HL-2M, the sensor signal noise is a sensitive issue, that need to be carefully taken into account when designing the RWM control system.

4. Conclusion and discussion

This work studies the $n = 1$ RWM control with plasma flow, magnetic feedback, and a combination of both on the HL-2M tokamak. As for the target plasma, we consider a high performance equilibrium with $I_p = 2$ MA, $B_0 = 2.2$ T and $\beta_N = 4.31\,(C_\beta = 0.4)$ designed for the AT scenario on HL-2M. Our primary goal is to take into account realistic control elements, i.e. the control power saturation and sensor signal noise issue, while quantifying various control parameters for the RWM.

Within the fluid model, which represents a conservative estimate for the RWM stability, we find that the subsonic plasma toroidal flow passively stabilizes the RWM only in a narrow region in the 2D parameter space $C_\beta - \Omega_0/\Omega_A$. The critical on-axis rotation frequency, for marginal stability of the RWM without feedback, is quantified via a linear fitting curve of $\Omega_0/\Omega_A = 0.152\ C_\beta$, as the plasma pressure varies.

Magnetic feedback can fully stabilize the RWM on HL-2M. Without considering the voltage limitation and the sensor signal noise, we find that plasma flow helps active control of the mode, by reducing the required critical feedback gain. This synergistic effect can be quantified by analytic fitting formulae $|G_{\rm cri}| = -38.6\,(\Omega_0/\Omega_A)^2 - 9.6\,\Omega_0/\Omega_A + 0.66$ for the flux-to-current control scheme, and $|G_{\rm cri}| = -47.9\ (\Omega_0/\Omega_A)^2 - 11.5\ \Omega_0/\Omega_A + 0.66$ for the flux-to-voltage control, based on the MARS-F computed eigenvalue results. These fitting formulae also confirm the analytic observation from equation (6), that the critical feedback gain is the same between the two control schemes at vanishing plasma flow.

MARS-F initial value simulations have also been carried out for the RWM feedback on HL-2M. In the absence of the sensor signal noise, the lowest control voltage saturation level, below which the RWM control is lost, is found to roughly satisfy a linear relation to the plasma flow frequency $V_f^{\min} = -1.08\ \Omega_0/\Omega_A + 0.054$ for the HL-2M target equilibrium, indicating that subsonic plasma flow is effective in relaxing the control power requirement for the RWM feedback stabilization.

The presence of the sensor signal noise substantially modifies the feedback results. Via statistical treatment, we find that the sensor signal noise, with the standard deviation of 0.1 G on HL-2M, roughly doubles the required control voltage (for successful mode control). The synergistic stabilization effect due to the plasma flow is somewhat weakened by the presence of the sensor signal noise. At a given rotation, the tolerable voltage limit generally increases with increasing feedback gain. At the toroidal rotation of $\Omega_0/\Omega_A = 0.02$, we find that the tolerable voltage limit at $|G| = 2$ is about twice of that at $|G| = 1$. This value (at $|G| = 2$) in turn is about four times larger than that without the sensor signal noise.

The above results offer useful guidance for future experiments on HL-2M. As mentioned before, in the later phase of operation, achieving high beta, high performance fusion plasmas is the key goal for HL-2M experiments. Both passive and active control methods are envisaged to control the RWM in high beta experiments. The computed critical plasma rotation speed to stabilize the RWM can be compared with experiments, helping to establish the damping roles played by the continuum wave resonances versus the particle drift resonances. The feedback gain amplitude and phase can be scanned in the RWM control experiments, with the optimal values compared with the modeling results. As mentioned earlier, more realistic conditions, such as the busbar resistance and other resistant elements in the control circuit, will increase the power required for the RWM control in real experiments. Comparison of the experimental results and simulations will be an important step in the HL-2M research program, not only to validate the present models, but also to pave ways for improving the models in view of providing even more reliable predictions for the future reactor scale devices such as China fusion engineering test reactor and ITER.

This work does not consider the derivative control action or other more advanced controller design. This remains a future study. The derivative action is not good when there is sensor noise, since taking time derivative will significantly amplify the sensor signal noise [31]. As a result, this may drastically increase the voltage and current needed in the active coils to control the RWM.

As discussed before, this work also neglected the drift kinetic stabilization effect on the RWM, due to thermal and/or energetic particles. This leads to conservative estimate of the passive stability of the mode on HL-2M. Thermal particle drift kinetic stabilization has been found to stabilize the RWM on HL-2M at slow toroidal flow ($\Omega_0 \leqslant 0.006\Omega_A$) [44]. The energetic particle effect, as well as the combined effect of both passive and active control in the presence of drift kinetic stabilization, will likely yield more optimistic results on the RWM stability on HL-2M, than what we have found here. Quantitative investigation remains a future work.

Data availability statement

The data that support the findings of this study are available upon reasonable request from the authors.

Acknowledgments

This work is supported by the National Natural Science Foundation of China (NSFC) under Grant No. 11805054. The work is also supported by the U.S. Department of Energy Office of Science under contracts DE-FG02-95ER54309 and DE-FC02-04ER54698. This work has been carried out within the framework of the EUROfusion Consortium and has received funding from the Euratom research and training programme 2014–2018 and 2019–2020 under Grant Agreement No. 633053. The views and opinions expressed herein do not necessarily reflect those of the European Commission.

ORCID iDs

S Wang https://orcid.org/0000-0001-6480-7004
Y Q Liu https://orcid.org/0000-0002-8192-8411
G Z Hao https://orcid.org/0000-0003-2310-6134
N Zhang https://orcid.org/0000-0003-3985-8031
G Q Dong https://orcid.org/0000-0002-4289-4060
X Bai https://orcid.org/0000-0002-0911-9935

References

[1] Hender T C *et al* 2007 *Nucl. Fusion* **47** S128
[2] Troyon F *et al* 1984 *Plasma Phys. Control. Fusion* **26** 209–15
[3] Bondeson A and Ward D 1994 *Phys. Rev. Lett.* **72** 2709
[4] Chu M S *et al* 1995 *Phys. Plasmas* **2** 2236
[5] Hu B and Betti R 2004 *Phys. Rev. Lett.* **93** 105002
[6] Sabbagh S *et al* 2006 *Nucl. Fusion* **46** 635
[7] Reimerdes H *et al* 2007 *Phys. Rev. Lett.* **98** 055001
[8] Takechi M *et al* 2007 *Phys. Rev. Lett.* **98** 055002
[9] Liu Y Q *et al* 2008 *Phys. Plasmas* **15** 112503
[10] Berkery J W *et al* 2010 *Phys. Plasmas* **17** 082504
[11] Hao G Z *et al* 2012 *Phys. Plasmas* **19** 032507
[12] He Y *et al* 2014 *Phys. Rev. Lett.* **113** 175001
[13] Liu C *et al* 2015 *Nucl. Fusion* **55** 063022
[14] Liu Y Q and Bondeson A 2000 *Phys. Rev. Lett.* **84** 907
[15] Liu Y Q *et al* 2000 *Phys. Plasmas* **7** 3681
[16] Fransson C M *et al* 2000 *Phys. Plasmas* **7** 4143
[17] Okabayashi M *et al* 2001 *Phys. Plasmas* **8** 2071
[18] Fredrickson E D *et al* 2001 *Plasma Phys. Control. Fusion* **43** 313
[19] Garfalo A *et al* 2001 *Nucl. Fusion* **41** 1171
[20] Fransson C M *et al* 2003 *Phys. Plasmas* **10** 3961
[21] Sen A K *et al* 2003 *Phys. Plasmas* **10** 4350
[22] Strait E J *et al* 2004 *Phys. Plasmas* **11** 2505
[23] In Y *et al* 2006 *Phys. Plasmas* **13** 062512
[24] Katsuro-Hopkins O *et al* 2007 *Nucl. Fusion* **47** 1157
[25] Hanson J M *et al* 2008 *Phys. Plasmas* **15** 080704
[26] Okabayashi M *et al* 2009 *Nucl. Fusion* **49** 125003
[27] Hanson J M *et al* 2009 *Phys. Plasmas* **16** 056112
[28] Wang Z *et al* 2011 *Nucl. Fusion* **51** 053004
[29] Li L *et al* 2012 *Phys. Plasmas* **19** 012502
[30] Wang S *et al* 2018 *Fusion Sci. Technol.* **73** 519
[31] Wang S *et al* 2019 *Nucl. Fusion* **59** 096021
[32] Brunsell P R *et al* 2004 *Phys. Rev. Lett.* **93** 225001
[33] Drake J R *et al* 2005 *Nucl. Fusion* **45** 557
[34] Brunsell P R *et al* 2005 *Plasma Phys. Control. Fusion* **47** B25
[35] Bolzonella T *et al* 2007 *Fusion Eng. Des.* **82** 1064–72
[36] Baruzzo M *et al* 2012 *Nucl. Fusion* **52** 103001
[37] Villone F *et al* 2008 *Phys. Rev. Lett.* **100** 255005
[38] Yadykin D *et al* 2011 *Plasma Phys. Control. Fusion* **53** 085024

[39] Li Q *et al* 2015 *Fusion Eng. Des.* **96–97** 338–42
[40] Li B *et al* 2019 *Fusion Eng. Des.* **147** 111229
[41] Xue L *et al* 2017 *Nucl. Fusion* **57** 056029
[42] Xia G L *et al* 2014 *Plasma Phys. Control. Fusion* **56** 095009
[43] Xia G L *et al* 2015 *Nucl. Fusion* **55** 093007
[44] Xia G L *et al* 2019 *Nucl. Fusion* **59** 016017
[45] Pustovitov V D 2002 *Plasma Phys. Control. Fusion* **44** 295
[46] Garofalo A M *et al* 2002 *Phys. Plasmas* **9** 4573
[47] Klein A J *et al* 2005 *Phys. Plasmas* **12** 040703
[48] Bondeson A and Chu M S 1996 *Phys. Plasmas* **3** 3013
[49] Liu Y Q *et al* 2004 *Nucl. Fusion* **44** 232–42
[50] La Haye R J *et al* 2004 *Nucl. Fusion* **44** 1197
[51] Bondeson A *et al* 2002 *Nucl. Fusion* **42** 768
[52] Liu Y Q 2007 *Comput. Phys. Commun.* **176** 161–9
[53] Liu Y Q *et al* 2017 *Fusion Sci. Technol.* **70** 387